Supporting Information

Egg Albumen Templated Graphene Foams for High-Performance Supercapacitor Electrodes and Electrochemical Sensors

Ya Liu,[a,b] Xiaoli Zhao,[a] Cancan Wang,[a] Long Zhang,[a] MengXiong Li,[a] Yunmei Pan,[a]

Hongbin Lu,[a,] and Johan Liu[b,c,*]*

[a]State Key Laboratory of Molecular Engineering of Polymers, Department of

Macromolecular Science, Collaborative Innovation Center of Polymers and Polymer

Composites, Fudan University, 2005 Songhu Road, Shanghai 200433, China,

[b]Electronics Materials and Systems Laboratory (EMSL), Department of

Microtechnology and Nanoscience (MC2), Chalmers University of Technology,

Kemivägen 9, SE-412 96 Göteborg, Sweden and [c]SMIT Center, Shanghai University,

No 20, Chengzhong Road, Shanghai, 201800, China.

Corresponding author. [a] *E- mail:* hongbinlu@fudan.edu.cn

[b,c]*E- mail: johan.liu@chalmers.se*

Table of Contents:

[14] **Table S2.** Elemental analysis (CNS) results of GF-800.

[15] **Table S3.** Comparison of supercapacitor performances for the samples in this study and the carbon-based materials from literature.

[16] **Table S4.** The specific electrochemical biosensors for detecting dopamine.

The Preparation procedures of Reduced Graphene Oxide (RGO): Firstly GO slurry suffer from suddenly frozen with liquid nitrogen and followed by freeze-drying for 2 days to form GO aerogel. Then the GO aerogel is transferred into tube furnace at 800 °C for 2 h. Before heating, the tube was purged with N_2 for 30 minutes, and the heating rate is set at 10 °C min^{-1}.
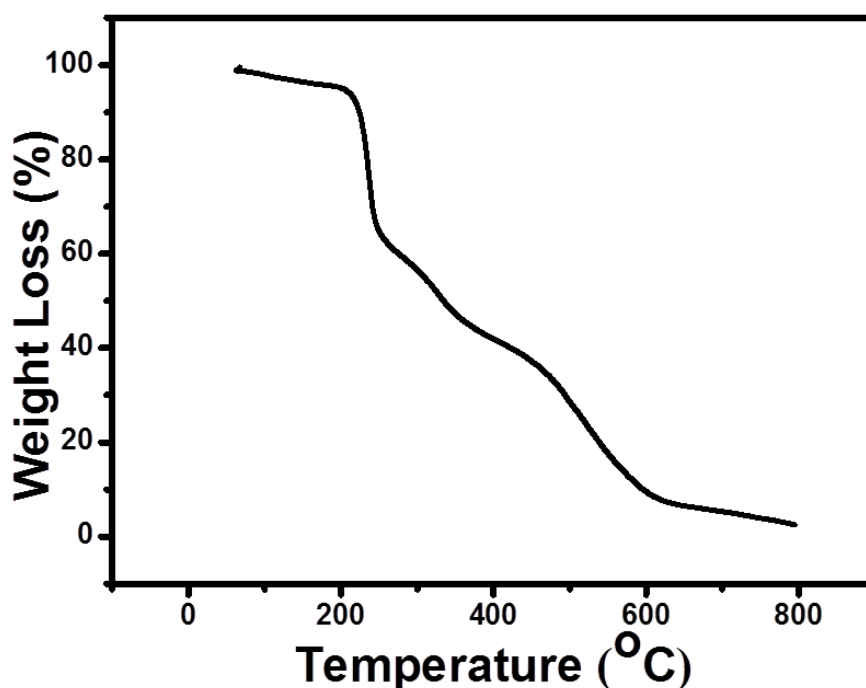
Fig. S1. Thermogravimetric analyses of egg albumen.

To further identify the components of GF, thermogravimetric analyses are performed to examine the thermal stability of egg albumen. Apparently, egg albumen is completely removed by pyrolysis with approximately 100% weight loss of TGA test.

Fig. S2. Raman spectra of (a) GO and GF; (b) GF-400, GF-600 and GF-800.

Fig. S3. SEM images of egg albumen foam with low (a) and high (b) magnifications.
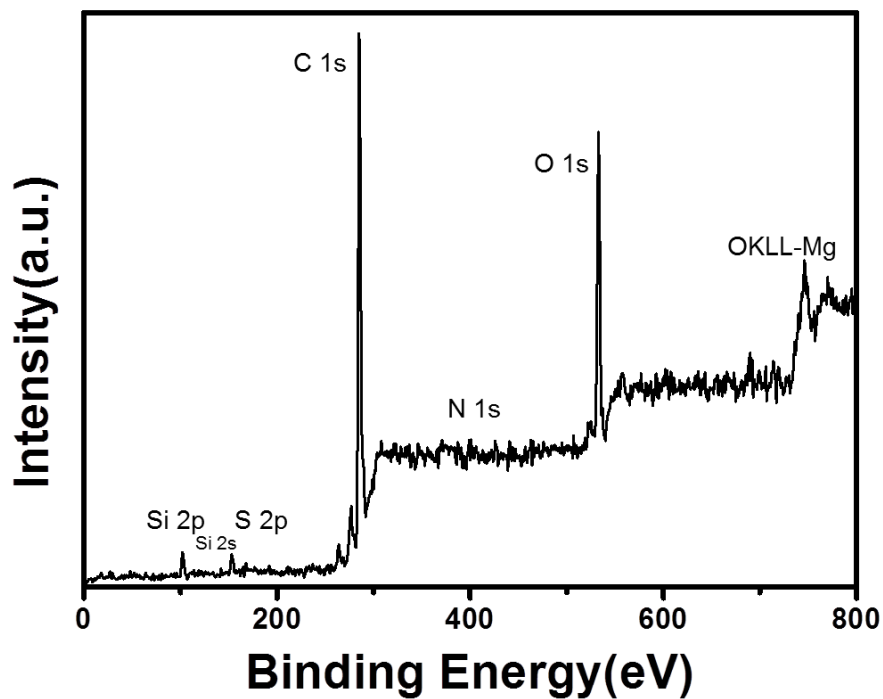
Fig. S4. XPS survey scan spectrum of obtained GF.
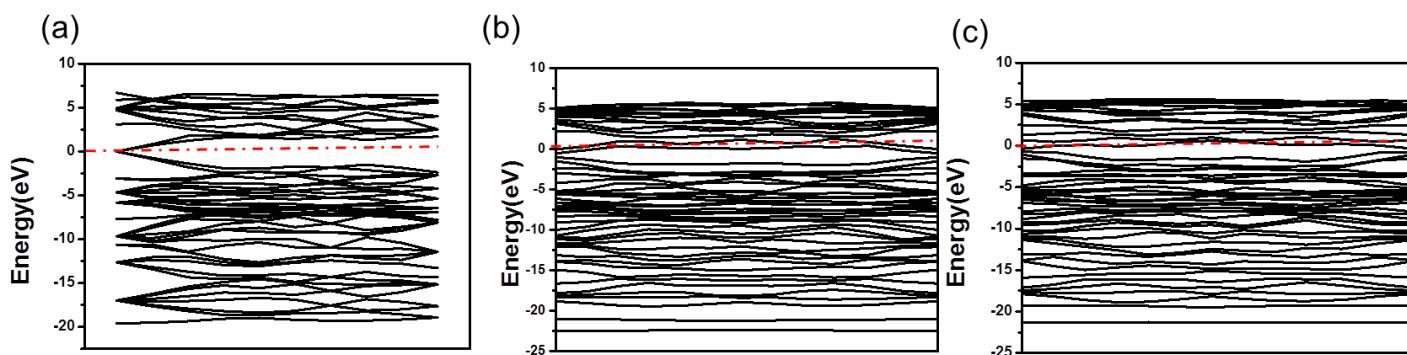
Fig. S5. The Band structures of (a) pristine graphene, (b) N, S, Si doped flawless

graphene, (c) N, S, Si doped defective graphene.
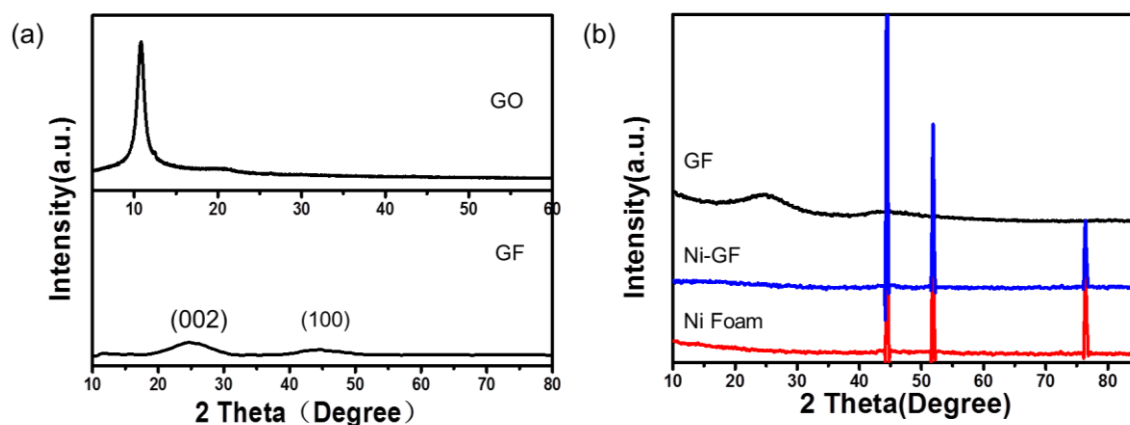
Fig. S6. XRD patterns of (a) GO and GF; (b) GF, Ni-GF and Ni-foam.

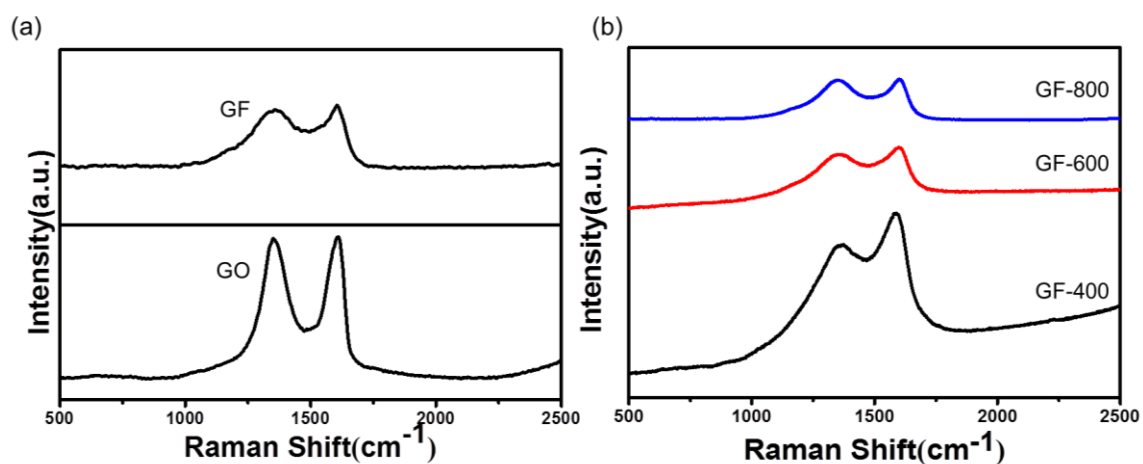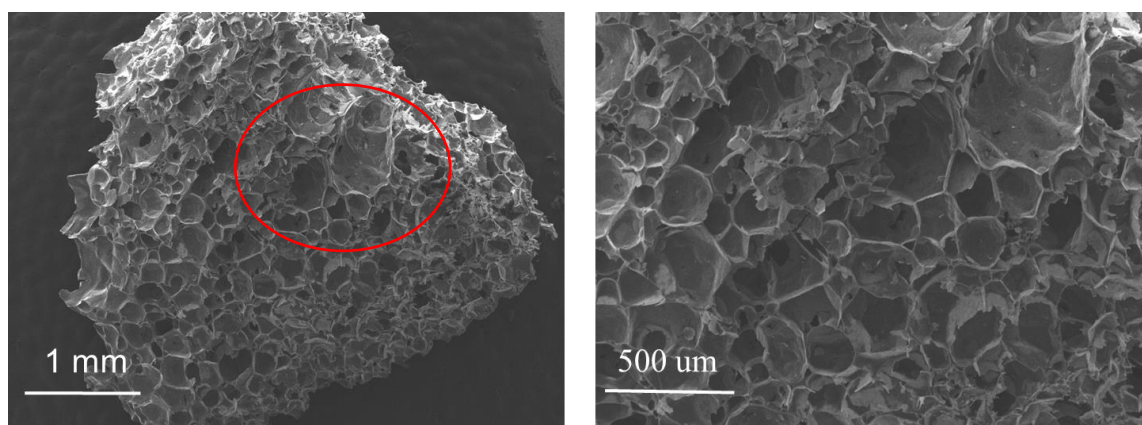XRD diffraction for GO, GF, Ni-foams (before and after annealing at 800°C) were carried out to verify where the capacitance comes from. The sharp diffraction peak at 10°, indicating pristine GO, disappears after thermal reduction at tube furnace suggesting that oxygen-containing groups have been removed in GF. Proverbially, two dominated broad and weak peaks of GF at position of $2\theta = 24°$ and $43°$ are attributed to (002) and (100) reflections of graphitic carbon layers, respectively. It is reported that porous structure and chemical doping are able to broaden peak width of (002). [1] After calcination, the peaks of Ni-foams match well with the peaks of original Ni-foams. This result confirms that Ni-foams keep stability during heating process. Thus we can exclude the contribution of Ni(OH)$_2$ to the capacitance.
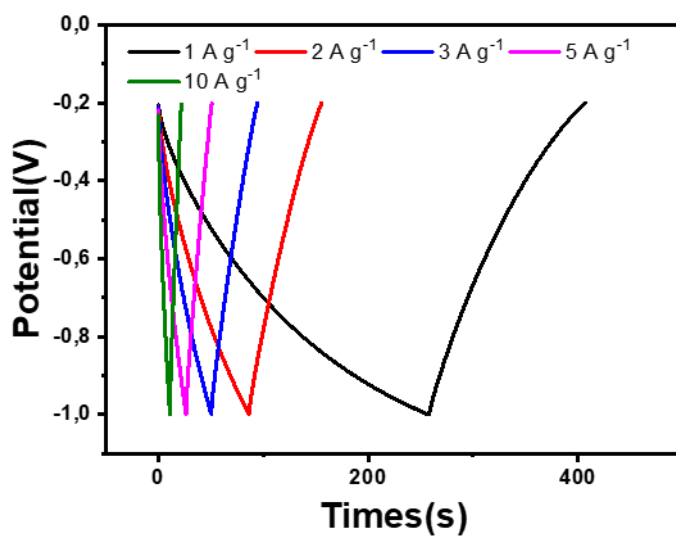
Fig. S7. Galvanostatic charging and discharging curves of RGO.
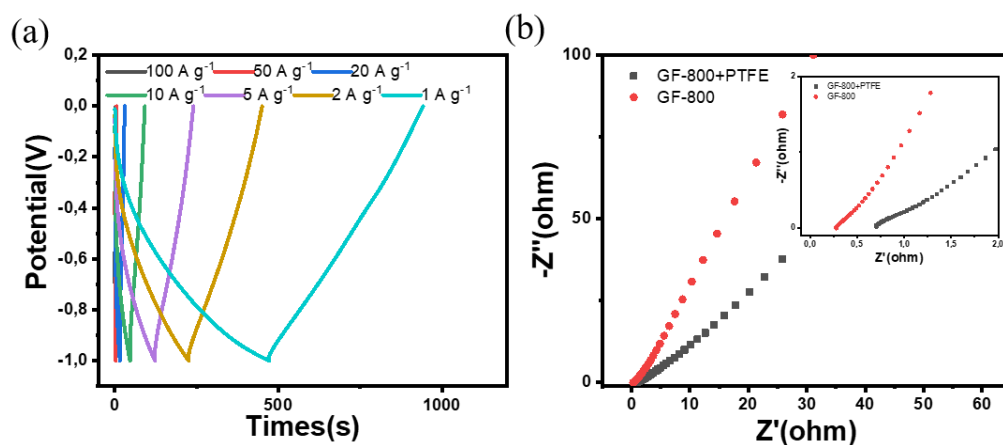
Fig. S8. (a) Galvanostatic charging and discharging curves of GF-800/PTFE. (b) Nyquist plots of GF-800/PTFE and GF-800; the inset shows the comparison at the high frequency region.
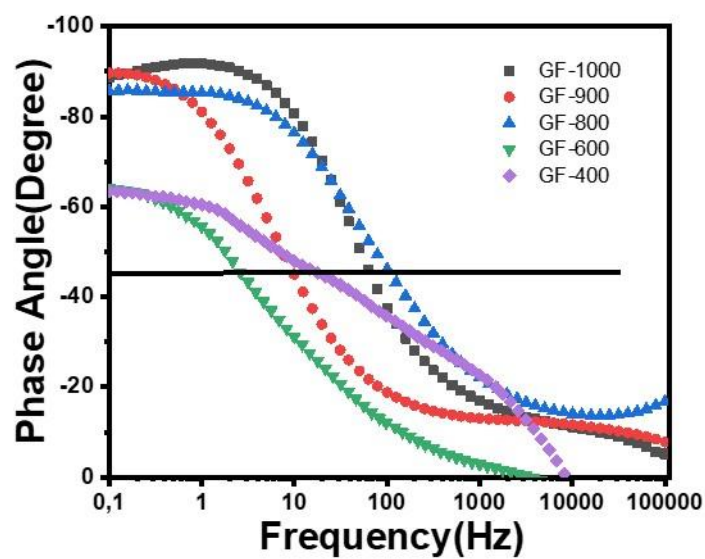
Fig. S9. Bode plots of phase angle versus frequency.

Table S1. Comparison of time constants for the samples in this study and the carbon-based materials from literature

Electrode materials	Time constant	Reference
GF-800	0.009	This Work
Multilayered Graphene Films	0.0133	2
Hierarchical Nitrogen-Doped Carbon Nanocages	0.39	3
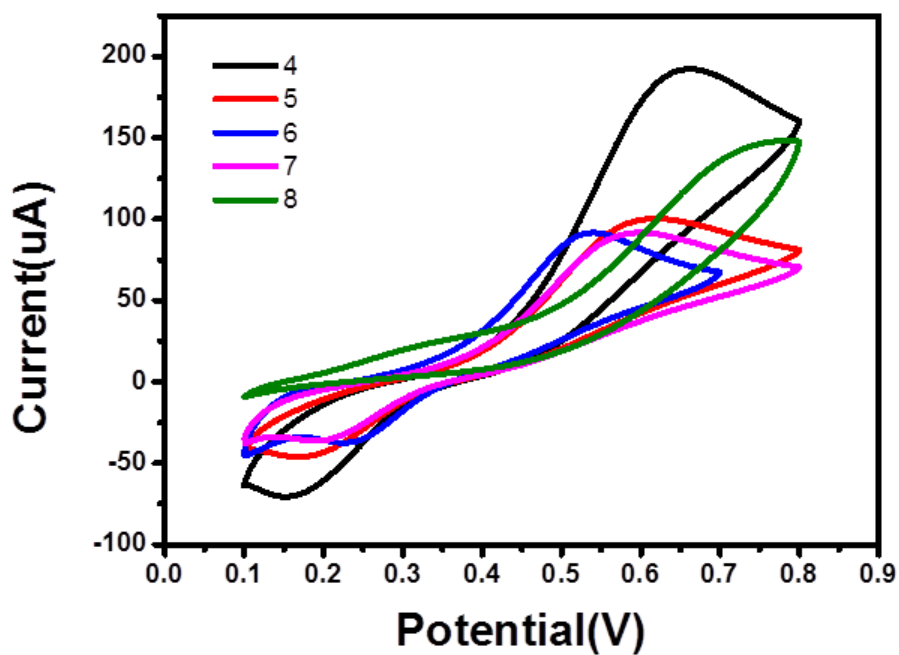
Fig. S10. CV curves of GF electrode in 0.1 M PBS solution with different pH values (4, 5, 6, 7, 8) with the presence of dopamine. Scan rate = 100 mV s^{-1}.

The pH dependence of DA with PBS solution is observed. Well-defined oxidation peaks can be observed when pH value ranging from 4 to 8, while redox peak disappear with the pH value increasing to 8 due to the deprotonation of hydroxyl groups of DA in alkali media, which consistent with reported results.
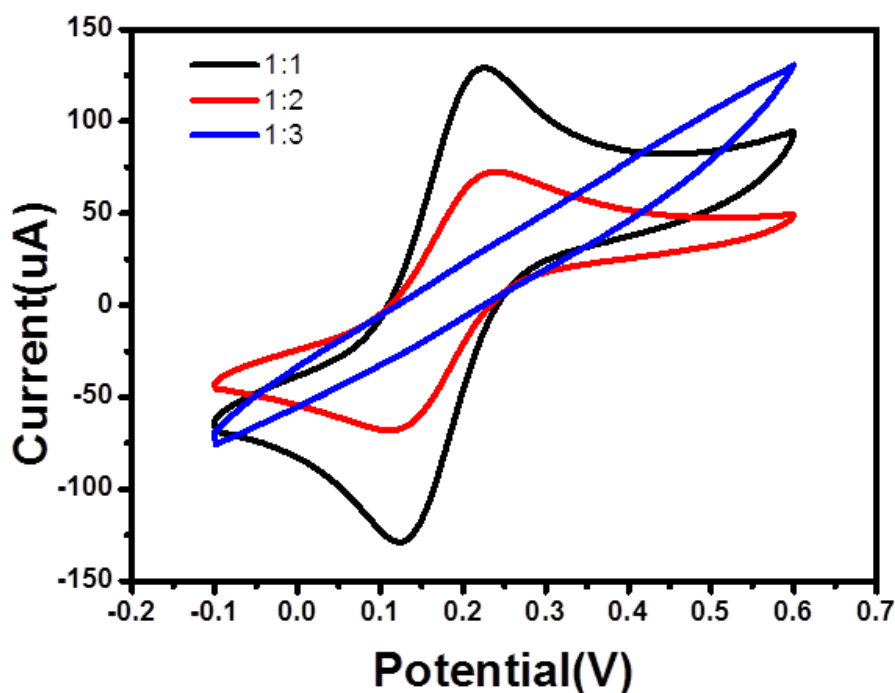
Fig. S11. CV curves of GF electrode in 0.1 M PBS solutions with different weight ratio of egg albumen and GO slurry (1:1, 1:2, 1:3) with the presence of dopamine. Scan rate = 100 mV s^{-1}.

Electrochemical sensing performance of different weight percentage of GF are studied and the 50% turn out to be the optimal weight ratio for GO slurry.

Table S2. Elemental analysis (CNS) results of GF-800.

Sample	N(%)	C(%)	S(%)
GF 800-1	4.9	78.59	0.31
GF 800-2	4.83	78.43	0.33

Table S3. Comparison of supercapacitor performances for the samples in this study

and the carbon-based materials from literature.

Electrode materials	BET SSA($m^2 g^{-1}$)	Cs($F g^{-1}$)/Current density($A g^{-1}$)	Rate capacity	Cycling stability	Reference
GF		534/1	58% (100A g^{-1})		This Study
N,S Co-Doped Graphene Hydrogel	-	536/5(mV s^{-1})	72% (100 mV s^{-1})	94.75% (7500, 4A g^{-1})	[4]
Hierarchical N-doped carbon nanocages	1794	313/1	75% (100A g^{-1})	98% (20000, 10A g^{-1})	[3]
Hierarchical Carbon	2582	401/5	87% (100 A g^{-1})	93% (4000,10A g^{-1})	[5]
Holey graphene frameworks	830	310/1	76% (100A g^{-1})	95% (20000,25A g^{-1})	[6]
Nitrogen and sulfur co-doped graphene nanoribbons	-	442/0.5	63% (10A g^{-1})	98.6% (10000, 2A g^{-1})	[7]
3D interconnected graphene nanocapsules	1985	277 /0.05	70% (25A g^{-1})	93% (15000, 2A g^{-1})	[8]
Sulfur and phosphorus co-doping of graphene	409	438 /10(mV s^{-1})	87% (500 mV s^{-1})	93.4% (10000, 1A g^{-1})	[9]
graphene aerogels	312	442/0.5	63% (10A g^{-1})	97.9% (10000, 2A g^{-1})	[10]
Nitrogen-Superdoped Graphene	583	380/0.6	63.2% (10A g^{-1})	93.5% (4600,5 A g^{-1})	[11]
3D Few-Layer Graphene-like Carbon	1545	231/1	56% (2000 A g^{-1})	99% (20000,1005A g^{-1})	[12]
ultrathin porous carbon shell	526	251/1	91% (20A g^{-1})	97% (10000, 3 A g^{-1})	[13]
Mesoporous nitrogen-rich carbons	800	390.4/0.25	68% (30A g^{-1})	93% (10000, 2 A g^{-1})	[14]
nonporous carbon nanofibers	-	243.7/0.5	83% (30A g^{-1})	>100% (8000, 30 A g^{-1})	[15]
3D printing graphene	436	57.5/0.5	65% (10A g^{-1})	-	[16]

Note: SSA: specific surface area, Cs: specific capacitance, -: not available.

Table S4. The specific electrochemical biosensors for detecting dopamine.

Sensors	Method	Detection limit/uM	Linear range/uM	Reference
GF	DPV	1.2	0.125-70	This Study
graphene ink	DPV	2.21	3–140	[17]
Au NPs/rGO/GCE	DPV	1.4	6.8–41	[18]

Hemin/GO/GCE	DPV	0.17	0.5–40	[19]
PEDOT modified LSG	DPV	0.33	1-150	[20]
N-2/Ar/GS/GNR	i-t	0.0025	0.01-400	[21]
Au-Cu_2O/rGO	DPV	0.0039	10-90	[22]
Co_3O_4/rGO/GCE	i-t	0.277	1-30	[23]
HNP-PtTi	DPV	-	0.000004-0.0005	[24]
pristine graphene	i-t	2	5-710	[25]
3D N-doped graphene	DPV	0.001	3-100	[26]

REFERENCES

1. Z. Xiong, C. Liao, W. Han and X. Wang, *Advanced Materials*, 2015, **27**, 4469-4475.

2. X. W. Yang, J. W. Zhu, L. Qiu and D. Li, *Advanced Materials*, 2011, **23**, 2833-+.

3. J. Zhao, H. W. Lai, Z. Y. Lyu, Y. F. Jiang, K. Xie, X. Z. Wang, Q. Wu, L. J. Yang, Z. Jin, Y. W. Ma, J. Liu and Z. Hu, *Advanced Materials*, 2015, **27**, 3541-3545.

4. N. Q. Tran, B. K. Kang, M. H. Woo and D. H. Yoon, *ChemSusChem*, 2016, **9**, 2261-2268.

5. J. Xu, Z. Tan, W. Zeng, G. Chen, S. Wu, Y. Zhao, K. Ni, Z. Tao, M. Ikram and H. Ji, *Advanced Materials*, 2016, **28**, 5222.

6. Y. Xu, Z. Lin, X. Zhong, X. Huang, N. O. Weiss, Y. Huang and X. Duan, *Nature Communications*, 2014, **5**, 4554.

7. K. Gopalsamy, J. Balamurugan, T. D. Thanh, N. H. Kim and J. H. Lee, 2017.

8. X. He, X. Li, H. Ma, J. Han, H. Zhang, C. Yu, N. Xiao and J. Qiu, *Journal of Power Sources*, 2017, **340**.

9. X. Yu, Y. Kang and H. S. Park, *Carbon*, 2016, **101**, 49-56.

10. S. M. Jung, D. L. Mafra, C. T. Lin, H. Y. Jung and J. Kong, *Nanoscale*, 2015, **7**, 4386-4393.

11. W. Zhang, C. Xu, C. Ma, G. Li, Y. Wang, K. Zhang, F. Li, C. Liu, H. M. Cheng and Y. Du, *Advanced Materials*, 2017, **29**.

12. J. Zhao, Y. Jiang, H. Fan, M. Liu, O. Zhuo, X. Wang, Q. Wu, L. Yang, Y. Ma and Z. Hu, *Advanced Materials*, 2017, **29**, 1604569.

13. W. Yang, F. Ding, G. Shao, L. Sang, W. Yang and Z. Ma, *Carbon*, 2017, **111**, 419-427.

14. Z. Li, Z. Xu, X. Tan, H. Wang, C. M. B. Holt, T. Stephenson, B. C. Olsen and D. Mitlin, *Energy & Environmental Science*, 2013, **6**, 871-878.

15. Y. Yang, X. Hou, C. Ding, J. Lan, Y. Yu and X. Yang, *Inorganic Chemistry Frontiers*, 2017.

16. C. Zhu, T. Liu, F. Qian, T. Y. Han, E. B. Duoss, J. D. Kuntz, C. M. Spadaccini, M. A. Worsley and Y. Li, *Nano Letters*, 2016, **16**, 3448.

17. L. Fu, A. W. Wang, G. S. Lai, W. T. Su, F. Malherbe, J. H. Yu, C. T. Lin and A. M. Yu, *Talanta*, 2018, **180**, 248-253.

18. C. Wang, P. Xu and K. Zhuo, *Electroanalysis*, 2014, **26**, 191-198.

19. H. L. Zou, B. L. Li, H. Q. Luo and N. B. Li, *Sensors & Actuators B Chemical*, 2015, **207**, 535-541.

20. G. Xu, Z. A. Jarjes, V. Desprez, P. A. Kilmartin and J. Travas-Sejdic, *Biosensors & bioelectronics*, 2018, **107**, 184-191.

21.   L. Jothi, S. Neogi, S. K. Jaganathan and G. Nageswaran, *Biosensors & Bioelectronics*, 2018, **105**, 236-242.

22.   T. K. Aparna, R. Sivasubramanian and M. A. Dar, *J. Alloy. Compd.*, 2018, **741**, 1130-1141.

23.   A. Numan, M. M. Shahid, F. S. Omar, K. Ramesh and S. Ramesh, *Sens. Actuator B-Chem.*, 2017, **238**, 1043-1051.

24.   D. Y. Zhao, G. L. Yu, K. L. Tian and C. X. Xu, *Biosensors & Bioelectronics*, 2016, **82**, 119-126.

25.   S. P. Qi, B. Zhao, H. Q. Tang and X. Q. Jiang, *Electrochimica Acta*, 2015, **161**, 395-402.

26.   X. M. Feng, Y. Zhang, J. H. Zhou, Y. Li, S. F. Chen, L. Zhang, Y. W. Ma, L. H. Wang and X. H. Yan, *Nanoscale*, 2015, **7**, 2427-2432.